THE JOURNAL OF PHYSICAL CHEMISTRY B

Article

pubs.acs.org/JPCB

pH Titration Monitored by Quantum Cascade Laser-Based Vibrational Circular Dichroism

Anja Rüther,[†] Marcel Pfeifer,[‡] Víctor A. Lórenz-Fonfría,[§] and Steffen Lüdeke*[,†]

[†]Institute of Pharmaceutical Sciences, Albert-Ludwigs-Universität Freiburg, Albertstr. 25, 79104 Freiburg, Germany

[‡]Fraunhofer Institute for Physical Measurement Techniques, Heidenhofstr. 8, 79110 Freiburg, Germany

[§]Experimental Molecular Biophysics, Freie Universität Berlin, Arnimallee 14, 14195 Berlin, Germany

Supporting Information

ABSTRACT: Vibrational circular dichroism (VCD) spectra of aqueous solutions of proline were recorded in the course of titrations from basic to acidic pH using a spectrometer equipped with a quantum cascade laser (QCL) as an infrared light source in the spectral range from 1320 to 1220 cm^{-1}. The pH-dependent spectra were analyzed by singular value decomposition and global fitting of a two-p*K* Henderson−Hasselbalch model. The analysis delivered relative fractions of the three different protonation species. Their agreement with the relative fractions obtained from performing the same analysis on pH-dependent Fourier transform infrared (FT-IR) and QCL-IR spectra validates the quantitative results from QCL-VCD. Global fitting of the pH-dependent VCD spectra of L-proline allowed for extraction of pure spectra corresponding to anionic, zwitterionic, and cationic L-proline. From a static experiment, only pure spectra of the zwitterion would be accessible in a straightforward way. A comparison to VCD spectra calculated for all three species led to assignment of vibrational modes that are characteristic for the respective protonation states. The study demonstrates the applicability of QCL-VCD both for quantitative evaluation and for qualitative interpretation of dynamic processes in aqueous solutions.

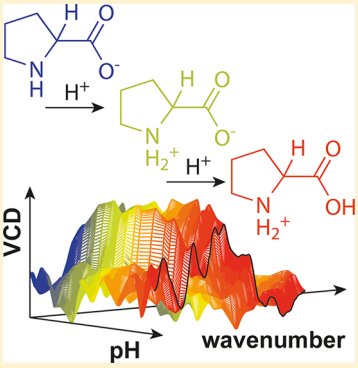

INTRODUCTION

Dynamic processes in biomolecules often involve proton transfer and therefore depend on pH. In proteins and peptides, pH dependence can be interpreted as the sum of contributions and interdependence of the p*K*s of individual amino acid residues leading to one or more global p*K*s of conformational transitions of the whole molecule.[1] These p*K*s might determine the pH conditions, for example, for protein folding,[2] enzyme activity,[3] or receptor activation.[4] Such transitions can be analyzed by monitoring pH-dependent changes of signals detected by a spectroscopic technique being sensitive for the process of interest.

The correlation between different species and pH can be approximated by the Henderson−Hasselbalch equation in analogy to the description of the pH dependence of protonation states of weak acids and bases:

$$\mathrm{pH} = \mathrm{p}K - \frac{[\mathrm{acid}]}{[\mathrm{base}]} \quad (1)$$

The Henderson−Hasselbalch relationship has been utilized for the description of different processes by fitting it to pH-dependent data obtained by various spectroscopic techniques, such as Fourier transform infrared (FT-IR),[5] UV/vis absorbance,[6] and electronic circular dichroism (ECD) spectroscopy.[6,7] In most of these examples, the p*K* was determined on the basis of the pH-dependent intensity of one or a few individual bands of the spectra. Technically speaking, the determined p*K* can be considered only the p*K* for a particular band and, thus, may not necessarily reflect the p*K* of the whole system. Therefore, it is desirable to fit full pH-dependent spectra, taking into account transition-related changes in different spectral regions.

Spectral contributions of different species in a three-dimensional data set can be either obtained from direct fitting of pure spectra or by applying deconvolution methods such as singular value decomposition (SVD), global fitting of amplitude spectra to model equations, or fitting methods combining both techniques.[8] The chiroptical methods ECD and vibrational circular dichroism (VCD) are particularly useful for such an approach because the positive and negative absorbance bands, reflecting the different absorbance of left and right circularly polarized light, are very sensitive toward conformational transitions.[9] Like IR spectra, VCD spectra reflect contributions of up to $3N - 6$ vibrational modes. These highly characteristic spectra allow for the reliable determination of the absolute configuration, which is the most common application of VCD.[10,11] Moreover, VCD also allows for the discrimination of different conformational structures in biological molecules.[12] With its high number of resolved spectral features VCD provides additional sensitivity compared to other spectroscopic methods and complements ECD for the assignment of

Received: December 16, 2013
Revised: March 21, 2014
Published: March 21, 2014

   dx.doi.org/10.1021/jp4122886 | J. Phys. Chem. B 2014, 118, 3941−3949

secondary structure.[13] Spectral shifts that indicate conformational changes are generally more distinct in the VCD than in the IR, which outweighs problems that arise from the low signal intensity in VCD ($\sim 10^{-4}$ × IR). However, IR and VCD spectroscopy of biological molecules is challenging due to the large background absorbance of water[14] that directly overlaps with the regions of interest.[12] This problem can be either partially circumvented by the use of D_2O instead of water as a solvent or by short path lengths (≤ 25 μm) to decrease the absorbance from water. Because the latter option comes at the cost of decreased signal intensities, spectral regions with an intrinsically weak magnitude of vibrational bands may be difficult to be studied by VCD spectroscopy. An example for such a spectral range is the amide III region of proteins and peptides (1400−1200 cm^{-1}), which features characteristic bands in Raman[15] but usually low intensity signals in the IR. Still, the amide III region could have a high potential as an IR probe for the secondary structure of peptides and proteins.[16] VCD data recorded in this spectral region could be used for assignment of secondary structure in protein and peptides, too, provided that the sample concentration was high enough to achieve sufficient signal intensities.[17]

Recently, it has been shown that use of a quantum cascade laser (QCL) as a light source allows for measuring of VCD samples with increased concentrations and path lengths, as demonstrated for VCD spectra of highly absorbent samples such as amino acids in water at a path length of 100 μm in the spectral range from 1320 to 1220 cm^{-1}.[18] The high output power of lasers provides new applications of VCD as a probe for dynamic processes as demonstrated with different types of lasers for different purposes: pump−probe systems for VCD measurements with ultrahigh time resolution,[19,20] an F-center ion laser for VCD-based chiral detection in liquid chromatography,[21] or QCL-VCD-based reaction monitoring.[22]

Like other spectroscopic techniques, VCD has been used for studies on pH-dependent processes in different kinds of biological molecules, including DNA analogues,[23] peptides,[24,25] proteins,[26−28] and single amino acids.[29,30] Most analyses of VCD spectra, recorded for pH-dependent processes, have been performed at single wavenumbers[14,23−26,29] and not by taking into account the full spectra, which would generate three-dimensional data, as required for chemometric analyses and reliable fitting of physical models. However, by analyzing two-dimensional VCD correlation spectra, such as of the amino acid L-alanine[30] or the protein α-lactalbumin,[27] it could be shown that the simultaneous evaluation of different VCD bands is a sensitive probe for pH-induced molecular changes. Multiple-wavelength analyses of VCD data have previously been used for studies on time-dependent processes, too, such as chemometric analyses in VCD-based time-dependent monitoring of enantiomeric excess[31−33] or global exponential fitting for the determination of kinetic parameters in the course of a QCL-VCD-monitored chemical reaction.[22]

As a model for dynamic processes of biological molecules, we titrated aqueous solutions of the amino acid proline between pH 11.4 and pH 2.0. Spectral changes monitored by the use of FT-IR, QCL-IR, and QCL-VCD spectroscopy corresponded to pH-dependent conversions between the different protonation species (Scheme 1). The resulting data were analyzed by a 3D global fitting procedure of a two-pK Henderson−Hasselbalch model and compared to the results obtained for the different methods. This study demonstrates the potential of QCL-VCD complementing FT-IR in the analysis of spectral changes

Scheme 1

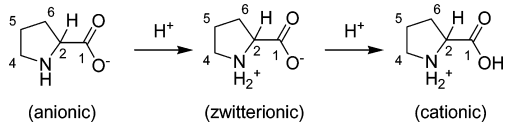

between 1320 and 1220 cm^{-1}, a range that has so far been largely neglected for the analysis of biological molecules.

The pH-dependent QCL-IR and VCD data were obtained by employing a fully automated flow-through titration setup. The 3D global fitting of the VCD data enabled us to extract VCD spectra of the pure anionic, zwitterionic, and also pure cationic species of L-proline. The latter cannot be easily recorded in aqueous solutions because a full protonation would require extremely acidic pH (pH −2 for 99.99% cationic proline). VCD bands that are characteristic for each species were assigned by a comparison to theoretical spectra calculated at the density functional theory (DFT) level.

EXPERIMENTAL METHODS

Titration of Proline. 1.035 g of L- or D-proline (Acros) was dissolved in 3 mL of a 2.5 M aqueous solution of NaOH in order to obtain a 3 M solution of proline. An automatic titrator (Titrino, Metrohm, Herisau, Switzerland), equipped with a pH-sensitive glass electrode, was used to set and measure pH values and to determine the volume of added HCl standard solution (2.5 M). For FT-IR measurements we prepared aliquots for every single pH value (11.76, 11.5 11.0, 10.5 10.0, 9.43, 8.79, 8.36, 7.18, 5.27, 3.73, 3.50, 3.00, 2.50, and 2.00), which were measured in CaF_2 cells with a path length either of 6 μm (sandwich-type micro cell) for an optimal signal-to-noise ratio in the spectral range from 1800 to 1000 cm^{-1} or of 25 μm for measurements from 1320 to 1220 cm^{-1}. The FT-IR molar absorptivities shown in Figures 2 and 4 were calculated using the individual concentration of each aliquot. For QCL-IR and QCL-VCD measurements the proline solution was automatically pumped (peristaltic pump P-1, GE Healthcare) through a 100 μm CaF_2 cell and measured after each titration step using a QCL-based spectrometer similar to the one described previously (Figure 1).[18] To ensure uniform pH in the whole setup (reaction vessel, cell, tubing), a LabVIEW routine was

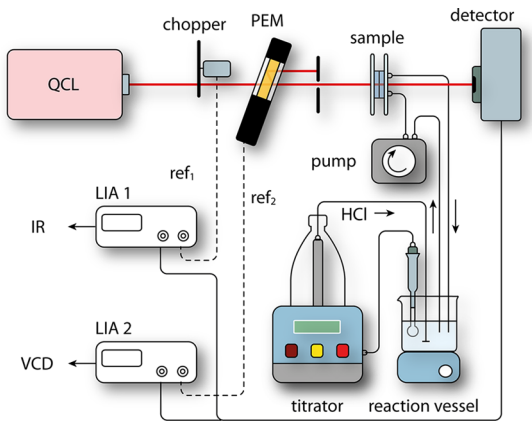

Figure 1. Experimental setup. QCL: external cavity quantum cascade laser; PEM: photoelastic modulator; LIA: lock-in amplifier; ref_1: frequency referenced to the chopper; ref_2: frequency referenced to the PEM.

dx.doi.org/10.1021/jp4122886 | J. Phys. Chem. B 2014, 118, 3941−3949

programmed, which involved two pumping/mixing cycles and automatic readjustment of the pH before each measurement was started. QCL-IR and QCL-VCD measurements of L-proline were undertaken at pH 11.36, 11.02, 10.54, 10.06, 9.55, 9.05, 8.52, 8.03, 7.52, 6.82, 6.20, 5.79, 4.85, 3.92, 3.49, 3.01, 2.53, and 2.03 (18 spectra incremented by ~0.5 pH value). IR intensities were modulated with a mechanical chopper and measured using a liquid N_2 cooled detector (L-8575 HCT-70, InfraRed Associates Inc., Stuart, FL). The laser output power was optimized for maximum signal intensity below detector saturation with respect to pure water background. Circularly polarized light was generated from the intrinsically linearly polarized laser beam with a photoelastic modulator (PEM 80, Hinds, Hillsboro, OR) with a frequency of 70 kHz and antireflective coating to suppress artifacts from laser interference. IR and VCD signals were obtained by two lock-in amplifiers (SR 830, Stanford Research Systems, Sunnyvale, CA) referenced to chopper and PEM frequencies, respectively. The step size of frequency scanning with the external cavity QCL (Daylight Solutions, San Diego, CA) was set to 0.5 cm^{-1} between 1320 and 1220 cm^{-1}, except for spectral bands from 1279 to 1272.5, 1255 to 1248, 1240 to 1235.5, and 1228 to 1222.5 cm^{-1}, where it was set to 0.25 cm^{-1}. The different step sizes were necessary in order to avoid gaps of >0.5 cm^{-1} between two sampling points, which arise after recalibration of nominal to actual frequencies (actual spectral range: 1322.5–1214.5 cm^{-1}) from inaccuracies in the frequency calibration of the laser. Different from previous setups for dispersive VCD using three lock-in amplifiers,[34−36] both lock-in amplifiers were set to the same time constant of 300 ms. To further improve the signal-to-noise ratio, each frequency data point was averaged over 20 lock-in readings taken in time intervals of 100 ms. The raw spectra were corrected for water background. Spectra in the range from 1320 to 1220 cm^{-1} (FT-IR, QCL-IR, and QCL-VCD) were baseline-corrected by applying a Fourier filter on each spectrum in order to remove frequency contributions of >100 cm^{-1}. QCL-IR and QCL-VCD spectra in Figures 3 and 4 were smoothed with a Fourier filter using Gaussian apodization for a final resolution of 5 cm^{-1}. Optical densities were converted into molar absorptivities by using individual concentrations c_n for each spectrum, calculated from the titrator volume readings v_n by $c_n = c_0 v_0/(v_0 + v_n)$.

Global Fitting. Global fitting of the pH-dependent VCD data set was performed using a two-pK Henderson–Hasselbalch equation, with the two pK values set constrained to 1.99 and 10.6.[37] The amplitude spectra were estimated using a singular value decomposition-based matrix least-squares method[8] in MATLAB (MathWorks, Natick, MA). Further details on the deconvolution of the spectral data including the SVD analysis that was performed prior to fitting are given in the Supporting Information.

Quantum Chemical Calculations. Conformers of anionic, zwitterionic, and cationic L-proline were modeled on the basis of previously published geometries of different ring-puckering conformers.[38−40] IR and VCD frequencies and intensities of anionic, zwitterionic, and cationic proline were calculated in GAUSSIAN 09[41] after geometry optimization at the B3LYP/6-311++G(d,p) level for each conformer, using the default PCM for water.[42] Frequencies were uniformly scaled by 0.98. Theoretical spectra for each geometry were obtained by adding Lorentzian band shapes (width: 6 cm^{-1}) to the calculated IR and VCD intensities.

RESULTS

Amino acids like proline have properties of both a weak acid and a weak base. Therefore, an algebraic equivalent to a two-pK Henderson–Hasselbalch equation using $pK_1 = 1.99$ and $pK_2 = 10.6$[37] for proline can be used as a good approximation for predicting the consumption of protons during the titration:

$$\frac{n_{H^+}}{n_{tot}} = \alpha\left(\frac{10^{pK_1-pH}}{1+10^{pK_1-pH}} + \frac{10^{pK_2-pH}}{1+10^{pK_2-pH}}\right) - \frac{n_0}{n_{tot}} \qquad (2)$$

Here n_0 is the molar amount of proline that is already protonated at the beginning of the titration (pH 11.4). The parameter α is a scaling factor that corrects for inaccuracies in the determination of the total molar amount of proline n_{tot} and can be determined by nonlinear fitting to the quantities corresponding to measured pH values. As expected, the relative consumptions for the different titration experiments are well described by eq 2, as shown for titration of L-proline, monitored by FT-IR in Figure 2A, and for titrations of L-proline and D-proline, monitored by QCL-IR and QCL-VCD in Figure 3A.

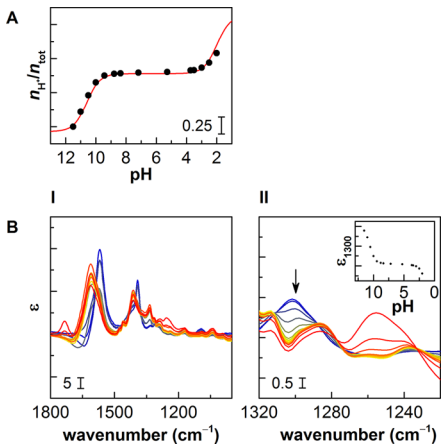

Figure 2. (A) Two-pK Henderson–Hasselbalch curves of H^+ consumption during the titration versus pH according to eq 2 fitted to values determined for L-proline used for FT-IR measurements (pK_1 = 1.99; pK_2 = 10.6; n_{tot} = 9.0 mmol; n_0 = 0.63 mmol; α = 0.85). (B) pH-dependent FT-IR spectra (corrected for water background and dilution effects) coded in litmus paper colors, from basic (blue), through neutral (green), to acidic (red) for the spectral range from 1800 to 1000 cm^{-1} recorded in a 6 μm cell (I) and from 1320 to 1220 cm^{-1} recorded in a 25 μm cell (II). In order to facilitate interpretation in this spectral region, all high bandwidth contributions were removed by Fourier filtering, which includes a pH-dependent tilt due to the low-frequency slope of the strong band at 1336 cm^{-1}. Inset: pH-dependent absorptivity at 1300 cm^{-1}.

Figure 2B(I) shows the pH-dependent FT-IR spectra corresponding to the pH values from Figure 2A in the spectral range from 1800 to 1000 cm^{-1} recorded in a 6 μm path length cell. The most prominent pH-dependent changes occur as a shift from 1570 to 1610 cm^{-1} upon transition from basic to acidic pH. The use of this spectral region alone for a quantitative analysis, however, is not recommendable because these bands overlap with a huge background band from bending vibration of water at 1644 cm^{-1}, which may be complicated by changing content of salt.[14] This becomes obvious from negative absorbance artifacts around 1650 cm^{-1} after background subtraction (Figure 2B(I)). In the range from 1500 to 1300 cm^{-1} there is a band shift (1392 to 1412 cm^{-1})

dx.doi.org/10.1021/jp4122886 | J. Phys. Chem. B 2014, 118, 3941−3949

and an increase in IR intensity at 1336 cm^{-1} that coincide with pH decrease. The spectral changes between 1320 and 1220 cm^{-1} are less intense but very clear and are spread over the whole pH range (Figure 2B(II)). For the measurement of these spectra we chose a 25 μm cell, which allowed for increased absorbance signals but still sufficient transmittance in the spectral range of interest. In the course of the titration a prominent IR absorbance maximum at 1300 cm^{-1}, observed at basic pH, splits into two maxima at 1310 and 1285 cm^{-1} at neutral pH. The pH-dependent increase in absorbance at 1300 cm^{-1} (Figure 2B, inset) is in accordance with a two-pK Henderson–Hasselbalch curve, similar to the one shown in Figure 2A. At acidic pH there is a significant increase in IR absorbance at 1255 cm^{-1}.

The molar absorptivity spectra in the range from 1320 to 1220 cm^{-1} from QCL-IR and QCL-VCD monitoring of the titration of L- and D-proline are shown in Figure 3B. QCL-VCD

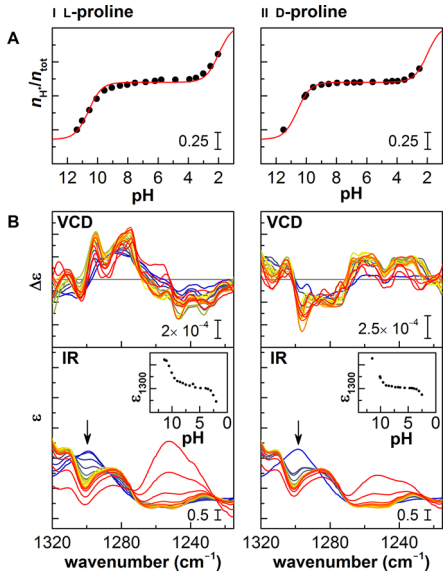

Figure 3. (A) Two-pK Henderson–Hasselbalch curves of H^+ consumption during the titration of L-proline (I) and D-proline (II) (pK_1 = 1.99; pK_2 = 10.6; n_{tot} = 9.0 mmol; n_0 = 1.3 mmol; α = 0.84). (B) Titration QCL-IR and QCL-VCD spectra measured for L-proline (left panel, I) and D-proline (right panel, II) at different pH values. All spectra are corrected for water background and baseline fluctuations and are smoothed by Fourier filtering (final resolution: 5 cm^{-1}). Insets: pH-dependent absorptivity at 1300 cm^{-1} plotted for L- (I) and D-proline (II).

spectra of D-proline recorded at the corresponding pH values as for L-proline appear as mirror-image spectra, while QCL-IR spectra for both enantiomers are identical and correspond well to the spectra measured by FT-IR spectroscopy in Figure 2B. In the VCD, pH-dependent spectral changes seem to manifest as changes of the whole spectral pattern rather than obvious changes in signal intensity at single wavelengths. The anisotropy ratio ($\Delta\varepsilon/\varepsilon$) of the pH-dependent spectral changes in the QCL-VCD with respect to the changes in the QCL-IR is about 10^{-4}, which is about the size of most VCD signals.[43] The strong QCL light source allows for measuring higher absorbent samples than FT-IR/VCD spectrometers in a comparable experiment. In the case of the titration of proline this is demonstrated by longer path lengths in QCL-IR/VCD experiments (100 μm) compared to the FT-IR experiments (25 μm for the same spectral range), which results in an increase of absolute signal intensity by a factor of 4. For a quantitative validation of the usefulness and reliability of QCL-VCD monitoring of spectral changes in the range from 1320 to 1220 cm^{-1}, we performed global fitting of the pH-dependent QCL-VCD data and compared the results to results from global fitting of QCL-IR and FT-IR data in the range from 1320 to 1220 cm^{-1} and FT-IR data in the range from 1800 to 1000 cm^{-1}.

Every spectrum at its individual pH value can be interpreted as a linear combination of spectral contributions from anionic, zwitterionic, and cationic proline. Contributions from the zwitterionic species dominate all spectra in the observed pH range (11.4–2.0). In order to quantify spectral contributions from each species and to extract the pure IR and VCD spectra corresponding to each species, we employed a model for global Henderson–Hasselbalch fitting of the pH-dependent QCL-VCD spectra. In analogy to eq 2, the ratio of anionic, zwitterionic, and cationic species can be approximated by two combined Henderson–Hasselbalch relationships:

$$A(\tilde{\nu}, \mathrm{pH}) = a_0(\tilde{\nu}) + a_1(\tilde{\nu})\frac{10^{pK_1-\mathrm{pH}}}{1 + 10^{pK_1-\mathrm{pH}}} + a_2(\tilde{\nu})\frac{10^{pK_2-\mathrm{pH}}}{1 + 10^{pK_2-\mathrm{pH}}} \quad (3)$$

Here, A is the data set of IR or VCD spectra recorded at different pH values. At infinite pH, the two Henderson–Hasselbalch terms (HHT) vanish. Therefore, a_0 is the spectrum that corresponds to deprotonated proline. The HHT-associated spectrum a_1 that refers to pK_1 (1.99) corresponds to the difference spectrum of cationic minus zwitterionic proline. The HHT-associated spectrum a_2 (pK_2 = 10.6) corresponds to zwitterionic minus anionic proline.

SVD of the titration data of L-proline suggested the existence of three significant spectral components (see Supporting Information, Figure S1). This is in agreement with the Henderson–Hasselbalch model for three protonation species (Scheme 1) given in eq 3 involving one pH-independent spectral component (a_0) and two HHT-related components (a_1 and a_2).

Figure 4 shows 3D plots of the experimental data sets measured for L-proline (upper panels of A–D) compared to the corresponding 3D plots of the fitted data using eq 3 with spectra a_0, a_1, and a_2 from global fitting (lower panels of A–D) for FT-IR in the range from 1800 to 1000 cm^{-1} (Figure 4A), FT-IR in the range from 1320 to 1220 cm^{-1} (Figure 4B), QCL-IR (Figure 4C), and QCL-VCD (Figure 4D). In particular, for the IR spectra the agreement with the model is excellent. Therefore, description of a pH titration of proline by a simple two-pK Henderson–Hasselbalch model seems to be valid. The experimental VCD data are subject to noise and baseline fluctuations. Still, the overall surface shape is very well described by eq 3 (Figure 4D). These findings show that QCL-VCD data in the range from 1320 to 1220 cm^{-1} can actually be used for quantitative chemometric analyses. This is further supported by comparison of the titration traces obtained from analyzing the data from FT-IR, QCL-IR, and QCL-VCD (Figure 5). The fractions correspond to the pH-dependent contribution of a pure spectrum, the spectrum that 100% of a protonation species would give, to every single pH-dependent spectrum. The pure IR (Supporting Information, Figure S3) and VCD spectra (Figure 6B) can be constructed

dx.doi.org/10.1021/jp4122886 | J. Phys. Chem. B 2014, 118, 3941–3949

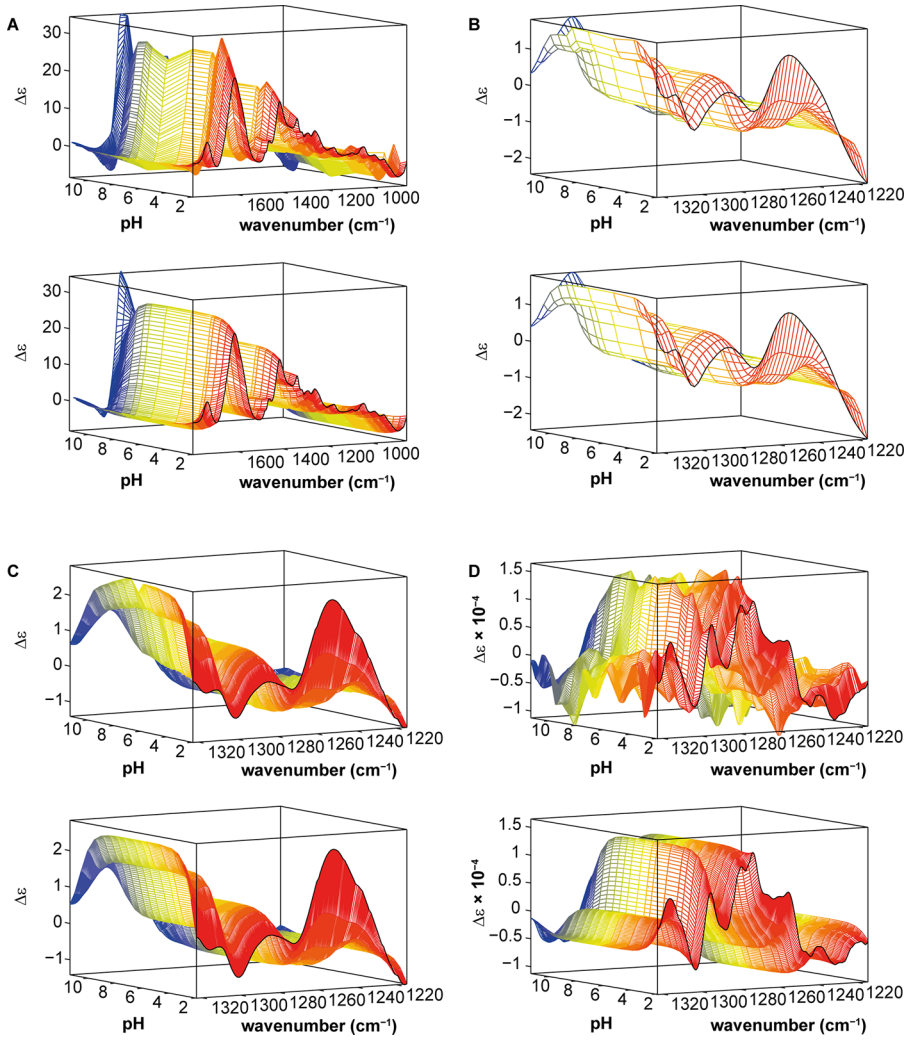

Figure 4. 3D plots of experimental spectral data of the pH titration of L-proline and 3D plots of the two-pK Henderson–Hasselbalch model using pK_1 = 1.99, pK_2 = 10.6, and amplitude spectra a_0, a_1, and a_2 obtained from global fitting to the respective spectra. (A) FT-IR data in the spectral range from 1800 to 1000 cm^{-1} (6 μm cell; background corrected). (B) FT-IR data in the spectral range from 1320 to 1220 cm^{-1} (25 μm cell; background- and baseline-corrected). (C) QCL-IR data in the spectral range from 1320 to 1220 cm^{-1}. (D) QCL-VCD data in the spectral range from 1320 to 1220 cm^{-1} (100 μm cell; both background- and baseline-corrected and smoothed to a final resolution of 5 cm^{-1}).

from the amplitude spectra a_0, a_1, and a_2 from global fitting. The fractions, calculated either from FT-IR or QCL-IR spectra or from QCL-VCD spectra, exhibit a pH-dependent curve progression that corresponds to a two-pK Henderson–Hasselbalch model. The deviations to theoretical curves calculated for pK_1 = 1.99 and pK_2 = 10.6 are comparable for all four experiments.

In order to test if the pure VCD spectra from global fitting in the range from 1320 to 1220 cm^{-1} could also be used for a qualitative assignment of the three proline species, we compared them to VCD spectra calculated for the anionic, zwitterionic, and cationic form at the B3LYP/6-311++G(d,p) level with a polarized continuum model (PCM) for water.[42] We used the calculated spectra to assign observed bands to vibrational modes of the two ring-puckering conformers A and B (shown in the Supporting Information, Figures S3–S5) that contribute to the theoretical spectra. In a conformational analysis of zwitterionic proline, including both potential energy surface calculations and NMR experiments, A and B have been identified as the two predominant conformers in a 50:50 ratio,[38] which is also in agreement with prior NMR studies.[44]

We modeled conformers for anionic proline based on geometries A and B and also geometries with different ring puckerings that had been suggested for anionic proline in gas-phase calculation studies.[39,40] However, after geometry optimization at the B3LYP/PCM/6-311++G(d,p) level, the two conformers with the ring puckering corresponding to A and B accounted for more than 99%, with a relative ratio A:B of 62:38, according to Boltzmann weights calculated with respect to their relative energies. Conformers of cationic proline were modeled by adding a hydrogen atom to the carboxylic acid moieties in A and B. Here, four conformers have to be taken into account because protonation of the carboxylic oxygen atom generates additional rotamers around the C1–O axis both in A and B (see Supporting Information, Figure S5). The ratios provided by the computational model were 280:1 for A_1:A_2 and 260:1 for B_1:B_2 and an overall relative ratio A:B of 44:56. Because experimental data for the conformational ratio in anionic and cationic proline are not available, the spectra in Figure 6C(I,III) were averaged weighted with the Boltzmann ratios given above.

dx.doi.org/10.1021/jp4122886 | J. Phys. Chem. B 2014, 118, 3941–3949

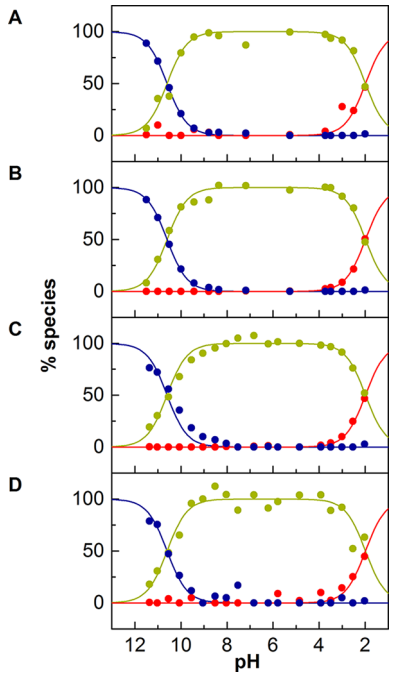

Figure 5. Fractions of pure VCD spectra in the pH-dependent experimental VCD spectra plotted against pH. The curves describe the theoretical normalized fraction of each species calculated with the respective Henderson–Hasselbalch terms and pK_1 = 1.99 and pK_2 = 10.6. (A) FT-IR data in the spectral range from 1800 to 1000 cm^{-1} (6 μm cell). (B) FT-IR data in the spectral range from 1320 to 1220 cm^{-1} (25 μm cell). (C) QCL-IR data in the spectral range from 1320 to 1220 cm^{-1}. (D) QCL-VCD data in the spectral range from 1320 to 1220 cm^{-1} (both 100 μm cell).

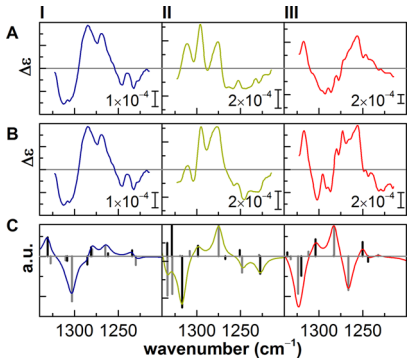

Figure 6. (A) VCD amplitude spectra a_0 (I), a_2 (II), and a_1 (III) from global fitting. (B) Pure VCD spectra for anionic (= a_0, I), zwitterionic (= a_0 + a_2, II), and cationic (= a_0 + a_1 + a_2, III) L-proline. (C) VCD spectra calculated at the B3LYP/6-311++G(d,p)/PCM level for anionic (I), zwitterionic (II), and cationic (III) proline. The weighted contributions of ring-puckering conformers are given by vertical lines (black: conformer A; gray: conformer B).

The good overall agreement of the experimental pure spectrum of anionic proline (Figure 6B(I)) and the spectra calculated for anionic conformers A and B (Figure 6C(I)) demonstrates that global fitting of a two-pK Henderson–Hasselbalch model delivers a reasonable VCD spectrum of proline in its fully deprotonated form. The positive signal in the pure spectrum of anionic proline at 1322 cm^{-1} (1331 cm^{-1} in the calculated spectrum) results from wagging of hydrogen atoms adjacent to the ring in conformer A. The broad negative signal at 1310 cm^{-1} (1303 cm^{-1} in the calculated spectrum) is predominantly caused by stretching vibrations of C2–C6 in conformer B. C2–H bending, wagging of ring hydrogens, and a weak bend of the carboxylate oxygens in both conformers lead to two positive signals at 1285 cm^{-1} (1281 cm^{-1}, conformer A) and 1269 cm^{-1} (1265 cm^{-1}, conformer B). For the zwitterionic species (Figure 6B(II)), the positive signal at 1310 cm^{-1} is not resolved in the calculated spectrum (Figure 6C(II)); it could be the result of skeletal vibrations of conformer B (calculated: 1308 cm^{-1}) but is canceled by a strong negative band (1316 cm^{-1} in the calculated spectrum) due to carboxylate bending and C–C stretching of C1 and C2 of conformer A. This is followed by two positive signals at 1296 and 1277 cm^{-1}; the former originates from wagging vibrations of conformer A (1299 cm^{-1}) and the latter from a bending of H–N–C2 in conformer B (1275 cm^{-1}). Vibrations correlated to C2–C6 stretching of conformer A (1251 cm^{-1}) appear as a small resolved feature at 1255 cm^{-1} in the pure spectrum. The two negative signals at 1246 and 1231 cm^{-1} derive from twisting and rocking of ring protons of conformers A (1248 cm^{-1}) and B (1227 cm^{-1}).

On first sight, the agreement between calculated and observed data for cationic proline is less obvious than for the anionic and the zwitterionic species. This could be due to inaccurate relative energies calculated for the conformers at the B3LYP/PCM/6-311++G(d,p) level. The pH-dependent change in IR absorbance (Figure 3B) shows a massive increase of a band between 1270 and 1220 cm^{-1}, which could well be explained by increasing contributions of C1–OH stretching vibrations in A_2 and B_2 (Figure 7). The corresponding

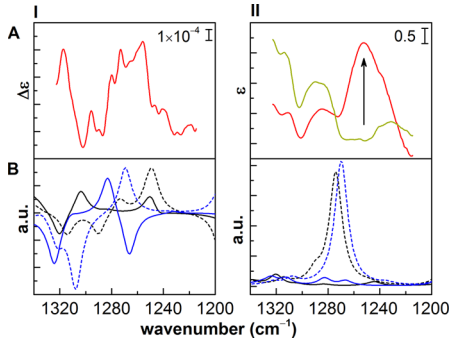

Figure 7. (A) Pure VCD spectrum (I) of cationic proline and IR absorbance (II) for spectra recorded at pH 6.20 (green) and 3.01 (red). (B) VCD (I) and IR (II) spectra calculated for conformers A_1 (solid black), A_2 (dashed black), B_1 (solid blue), and B_2 (dashed blue). A strong IR absorbance at around 1260 cm^{-1} is predicted for conformers A_2 (dashed black) and B_2 (dashed blue), but not for A_1 (solid black) and B_1 (solid blue).

vibrations in A_1 and B_1 would both cause absorbance bands at 1151 cm^{-1}, which is outside the observed spectral range. This suggests an underestimated population of A_2 and B_2. Nevertheless, taking into account spectral contributions from all four conformers (Figure 7) allows for assignment of VCD bands in cationic proline, too. The VCD spectrum shows a noticeable positive doublet at 1274 and 1256 cm^{-1} that corresponds to the strong IR absorbance and can therefore be assigned to C1–OH stretch vibrations of A_2 (1249 cm^{-1}) and B_2 (1270 cm^{-1}) and possible contributions of H–N–C2 bending in B_1 (1283 cm^{-1}). The negative doublet at 1303 and 1288 cm^{-1} may comprise contributions from O=C1–OH bending of the carboxylic acid moiety in A_1 (1320 cm^{-1}) and C1–C2 and

dx.doi.org/10.1021/jp4122886 | J. Phys. Chem. B 2014, 118, 3941–3949

C2−C6 stretching and corresponding skeletal vibrations of both B_1 (1324 cm^{-1}) and B_2 (1308 cm^{-1}). Negative contributions from A_2 appear at lower frequencies (1314 and 1290 cm^{-1}) than those mentioned above and are less intense.

DISCUSSION

Global fitting of three-dimensional data sets allows for extracting or, in the case of proline, extrapolating to spectra that are difficult to obtain by means of a static experiment. The decomposition of the spectral data into pure components corresponding to molecular species, however, requires characteristic spectral changes being invoked by the perturbation that is made to the system, here the decrease in pH. The significance of spectral changes depends on the choice of spectroscopic method that is used to observe them. For studying chiral biological molecules chiroptical methods often provide additional information compared to absorbance spectroscopy. The pH dependence of ECD spectra of different amino acids has been described previously, in the case of proline being mainly reflected in different signal intensities and slight frequency shifts.[45] The VCD of amino acids, on the other hand, may exhibit considerable spectral changes concomitant with shifting between basic and acidic conditions in different spectral ranges, as shown previously for the titration of L-alanine, analyzed by two-dimensional VCD correlation spectroscopy.[30] As shown above, the IR spectra of proline around neutral pH exhibit two dominant signals at 1310 and 1285 cm^{-1}, which are not present at basic pH. These signals correspond to bending vibrations of the additional hydrogen atom, after protonation of the amino group, in the two conformers of zwitterionic proline. Spectral changes between neutral and acidic pH are dominated by a huge increase in absorbance between 1270 and 1220 cm^{-1}, which we attribute to C1−OH stretching vibrations that do only occur in the protonated species. VCD, however, is also sensitive to pH-dependent changes in bending vibrations of the whole scaffold and adjacent hydrogen atoms, which leads to change of the whole spectral pattern between basic, neutral, and acidic pH. The spectral features specifically observed for IR and VCD spectra of protonated L-proline cannot be assigned by using Boltzmann-weighted spectra calculated at the B3LYP/6-311++G(d,p) level with a polarized continuum model for water. The mismatch in agreement between the calculated and observed spectra is clearly due to inaccurate conformer weights with respect to relative energies obtained from the DFT calculations. Therefore, QCL-based IR and VCD measurements in the spectral range from 1320 to 1220 cm^{-1}, being so far largely neglected for the analysis of charged chiral molecules in water, may serve as a benchmark for the development of improved solvation models for water.

The fraction of different protonation states in proline can be approximated by a two-p*K* Henderson−Hasselbalch model. According to this model, fully deprotonated proline (99.99%) would exist at pH 14.6, while formation of 99.99% cationic proline would require pH −2.0, a value that cannot easily be established in aqueous solutions. Although the interdependence between the two p*K*s may not be described accurately over the full pH range,[46] the two-p*K* Henderson−Hasselbalch model is still a good enough approximation for obtaining pure spectra of protonation species to allow for assignment of bands to vibrational modes by comparison to calculated spectra. Because global fitting incorporates spectral information from the full three-dimensional data set, the quality of the fitted spectra and/or parameters depends on both the accuracy of single data points and on the number of data points in the direction of the axis of progression (here: pH). The performance of regression methods in general increases with the size of the data set.[47] As a consequence, for experiments such as titrations an automated setup is recommended in order to obtain a reasonable number of data points. The reliability of the global fit of a 3D spectral data set also increases with the number of data points in the direction of the frequency axis, in particular if more than two species are involved that may have spectral contributions in different spectral regions. Because of the high content of information with a large number of narrow signals, vibrational spectroscopy methods, such as IR or VCD, are ideally suited for multiple-wavelength analyses. Many IR and VCD studies on aqueous solutions of biological molecules monitor signals in the spectral range from 1700 to 1300 cm^{-1}. The extension to the range below 1300 cm^{-1} may add spectral information but is usually hampered by low signal intensities in this spectral region compared to a strong background from water. Increasing the signal intensity by increasing the concentration and/or the path length is in most cases not an option for FT-IR and FT-VCD because the incandescent light sources generally used in these instruments are too weak for sufficient transmission of IR light through highly absorbent samples. The use of a QCL light source allows for measuring VCD signals and for their qualitative and quantitative analysis of aqueous samples in a spectral range, in which FT-VCD experiments are traditionally difficult.

CONCLUSIONS

Because the concept of pH is intrinsically defined for water, and biological molecules usually exist in an aqueous environment, monitoring the pH dependence of biochemical processes only makes sense in aqueous solutions. Because of the large background absorbance of water, however, such systems are difficult to handle in IR or VCD spectroscopy. D_2O is a widely used substitute for water. It shifts the problem of background interference from the solvent to lower frequencies and has better optical properties than water in the spectral range that has been used for most IR and VCD studies on biological molecules, including pD-dependent changes in the VCD spectra of peptides (e.g., poly(L-proline)).[25] For the interpretation of vibrational spectra, isotopic effects from deuterium on the vibrational modes have to be taken into account, which often is ambiguous due to incomplete H/D exchange.[48] VCD studies on aqueous solutions usually require short path lengths, rendering smaller signals undetectable.[29] Furthermore, the use of short path lengths may result in technical problems in reaction monitoring involving flow-through devices. We have shown that these problems can be overcome with QCL-VCD, which allows for the measurement of spectra of highly absorbing samples using a reasonable path length (100 μm). As shown for the titration of L-proline, QCL-VCD spectra in the spectral range from 1320 to 1220 cm^{-1} can be used for global fitting of physical models to three-dimensional data sets, which results in the same quantitative results as obtained from global fitting of FT-IR spectra of the same or a broader spectral range from 1800 to 1000 cm^{-1}. A similar setup could also be used for more complex pH-sensitive systems, such as proteins or peptides, thereby verifying the models describing the pH-dependent conversions on one hand and, on the other hand, allowing for the identification of the involved intermediates by extracting the corresponding spectra.

dx.doi.org/10.1021/jp4122886 | J. Phys. Chem. B 2014, 118, 3941−3949

■ ASSOCIATED CONTENT

Supporting Information

Details on the SVD and fitting analysis of experimental data and on the conformers used for quantum chemical calculations. This material is available free of charge via the Internet at http://pubs.acs.org.

■ AUTHOR INFORMATION

Corresponding Author

*E-mail steffen.luedeke@pharmazie.uni-freiburg.de; Tel +49 (0)761 203-6353; Fax +49 (0)761 203-6351 (S.L).

Notes

The authors declare no competing financial interest.

■ ACKNOWLEDGMENTS

The authors thank Dr. A. Lambrecht for the loan of the QCL and Prof. M. Müller and Prof. P. Fischer for helpful discussions. We acknowledge the use of the computing resources provided by the Black Forest Grid Initiative. S.L. is indebted to the Baden-Württemberg Stiftung for financial support of this research project through the Elite Programme for Postdoctoral Fellows.

■ REFERENCES

(1) Matthew, J. B.; Gurd, F. R. N.; Garciamoreno, E. B.; Flanagan, M. A.; March, K. L.; Shire, S. J. pH-Dependent Processes in Proteins. *CRC Crit. Rev. Biochem.* **1985**, *18*, 91−197.

(2) Oliveberg, M.; Fersht, A. R. Formation of Electrostatic Interactions on the Protein-Folding Pathway. *Biochemistry* **1996**, *35*, 2726−2737.

(3) Tipton, K. F.; Dixon, H. B. F.; Daniel, L. P. Effects of pH on Enzymes. *Methods Enzymol.* **1979**, *63*, 183−234.

(4) Matthews, R. G.; Wald, G.; Brown, P. K.; Hubbard, R. Tautomeric Forms of Metarhodopsin. *J. Gen. Physiol.* **1963**, *47*, 215−240.

(5) Vogel, R.; Fan, G. B.; Siebert, F.; Sheves, M. Anions Stabilize a Metarhodopsin II-Like Photoproduct with a Protonated Schiff Base. *Biochemistry* **2001**, *40*, 13342−13352.

(6) Konkle, M. E.; Muellner, S. K.; Schwander, A. L.; Dicus, M. M.; Pokhrel, R.; Britt, R. D.; Taylor, A. B.; Hunsicker-Wang, L. M. Effects of pH on the Rieske Protein from *Thermus thermophilus*: A Spectroscopic and Structural Analysis. *Biochemistry* **2009**, *48*, 9848−9857.

(7) Durell, S. R.; Gross, E. L.; Draheim, J. E. Analysis of the Near-Ultraviolet Absorption and Circular Dichroic Spectra of Parsley Plastocyanin for the Effects of pH and Copper Center Conformation Changes. *Arch. Biochem. Biophys.* **1988**, *267*, 217−227.

(8) Shrager, R. I.; Hendler, R. W. Titration of Individual Components in a Mixture with Resolution of Difference Spectra, pKs, and Redox Transitions. *Anal. Chem.* **1982**, *54*, 1147−1152.

(9) Berova, N., Polavarapu, P. L., Nakanishi, K.; Woody, R. W., Eds.; *Comprehensive Chiroptical Spectroscopy*; John Wiley & Sons., Inc.: Hoboken, NJ, 2012; Vol. 2.

(10) Freedman, T. B.; Cao, X. L.; Dukor, R. K.; Nafie, L. A. Absolute Configuration Determination of Chiral Molecules in the Solution State Using Vibrational Circular Dichroism. *Chirality* **2003**, *15*, 743−758.

(11) Stephens, P. J.; Devlin, F. J.; Pan, J.-J. The Determination of the Absolute Configurations of Chiral Molecules Using Vibrational Circular Dichroism (VCD) Spectroscopy. *Chirality* **2008**, *20*, 643−663.

(12) Keiderling, T. A. Conformational Studies of Biopolymers, Peptides, Proteins, and Nucleic Acids. A Role for Vibrational Circular Dichroism. In *Comprehensive Chiroptical Spectroscopy*; Berova, N., Polavarapu, P. L., Nakanishi, K., Woody, R. W., Eds.; John Wiley & Sons, Inc.: Hoboken, NJ, 2012; Vol. 2, pp 707−758.

(13) Pancoska, P.; Bitto, E.; Janota, V.; Urbanova, M.; Gupta, V. P.; Keiderling, T. A. Comparison of and Limits of Accuracy for Statistical Analyses of Vibrational and Electronic Circular Dichroism Spectra in Terms of Correlations to and Predictions of Protein Secondary Structure. *Protein Sci.* **1995**, *4*, 1384−1401.

(14) Venyaminov, S. Y.; Prendergast, F. G. Water (H_2O and D_2O) Molar Absorptivity in the 1000−4000 cm^{-1} Range and Quantitative Infrared Spectroscopy of Aqueous Solutions. *Anal. Biochem.* **1997**, *248*, 234−245.

(15) Asher, S. A.; Ianoul, A.; Mix, G.; Boyden, M. N.; Karnoup, A.; Diem, M.; Schweitzer-Stenner, R. Dihedral ψ Angle Dependence of the Amide III Vibration: A Uniquely Sensitive UV Resonance Raman Secondary Structural Probe. *J. Am. Chem. Soc.* **2001**, *123*, 11775−11781.

(16) Cai, S. W.; Singh, B. R. A Distinct Utility of the Amide III Infrared Band for Secondary Structure Estimation of Aqueous Protein Solutions Using Partial Least Squares Methods. *Biochemistry* **2004**, *43*, 2541−2549.

(17) Baello, B. I.; Pancoska, P.; Keiderling, T. A. Vibrational Circular Dichroism Spectra of Proteins in the Amide III Region: Measurement and Correlation of Bandshape to Secondary Structure. *Anal. Biochem.* **1997**, *250*, 212−221.

(18) Lüdeke, S.; Pfeifer, M.; Fischer, P. Quantum-Cascade Laser-Based Vibrational Circular Dichroism. *J. Am. Chem. Soc.* **2011**, *133*, 5704−5707.

(19) Bonmarin, M.; Helbing, J. A Picosecond Time-Resolved Vibrational Circular Dichroism Spectrometer. *Opt. Lett.* **2008**, *33*, 2086−2088.

(20) Rhee, H. J.; June, Y. G.; Lee, J. S.; Lee, K. K.; Ha, J. H.; Kim, Z. H.; Jeon, S. J.; Cho, M. H. Femtosecond Characterization of Vibrational Optical Activity of Chiral Molecules. *Nature* **2009**, *458*, 310−313.

(21) Tran, C. D.; Grishko, V. I.; Huang, G. L. Chiral Detection in High-Performance Liquid-Chromatography by Vibrational Circular Dichroism. *Anal. Chem.* **1994**, *66*, 2630−2635.

(22) Rüther, A.; Pfeifer, M.; Lórenz-Fonfría, V. A.; Lüdeke, S. Reaction Monitoring Using Mid-Infrared Laser-Based Vibrational Circular Dichroism. *Chirality* **2014**, DOI: 10.1002/chir.22307.

(23) Petrovic, A. G.; Polavarapu, P. L. Structural Transitions in Polyriboadenylic Acid Induced by the Changes in pH and Temperature: Vibrational Circular Dichroism Study in Solution and Film States. *J. Phys. Chem. B* **2005**, *109*, 23698−23705.

(24) Zuk, W. M.; Freedman, T. B.; Nafie, L. A. Vibrational CD Studies of the Solution Conformation of Simple Alanyl Peptides as a Function of pH. *Biopolymers* **1989**, *28*, 2025−2044.

(25) Dukor, R. K.; Keiderling, T. A. Reassessment of the Random Coil Conformation: Vibrational CD Study of Proline Oligopeptides and Related Polypeptides. *Biopolymers* **1991**, *31*, 1747−1761.

(26) Yasui, S. C.; Pancoska, P.; Dukor, R. K.; Keiderling, T. A.; Renugopalakrishnan, V.; Glimcher, M. J.; Clark, R. C. Conformational Transitions in Phosvitin with pH Variation - Vibrational Circular Dichroism Study. *J. Biol. Chem.* **1990**, *265*, 3780−3788.

(27) Ryu, S. R.; Czarnik-Matusewicz, B.; Dukor, R. K.; Nafie, L. A.; Jung, Y. M. Analysis of the Molten Globule State of Bovine α-Lactalbumin by Using Vibrational Circular Dichroism. *Vib. Spectrosc.* **2012**, *60*, 68−72.

(28) Xu, Q.; Keiderling, T. A. Optical Spectroscopic Differentiation of Various Equilibrium Denatured States of Horse Cytochrome c. *Biopolymers* **2004**, *73*, 716−726.

(29) Poopari, M. R.; Zhu, P. Y.; Dezhahang, Z.; Xu, Y. J. Vibrational Absorption and Vibrational Circular Dichroism Spectra of Leucine in Water under Different pH Conditions: Hydrogen-Bonding Interactions with Water. *J. Chem. Phys.* **2012**, 137 DOI: 10.1063/1.4767401.

(30) Ma, S. L.; Freedman, T. B.; Cao, X. L.; Nafie, L. A. Two-Dimensional Vibrational Circular Dichroism Correlation Spectroscopy: pH-Induced Spectral Changes in L-Alanine. *J. Mol. Struct.* **2006**, *799*, 226−238.

(31) Guo, C. N.; Shah, R. D.; Dukor, R. K.; Cao, X. L.; Freedman, T. B.; Nafie, L. A. Determination of Enantiomeric Excess in Samples of Chiral Molecules Using Fourier Transform Vibrational Circular Dichroism Spectroscopy: Simulation of Real-Time Reaction Monitoring. *Anal. Chem.* **2004**, *76*, 6956−6966.
(32) Guo, C. N.; Shah, R. D.; Dukor, R. K.; Cao, X. L.; Freedman, T. B.; Nafie, L. A. Enantiomeric Excess Determination by Fourier Transform Near-Infrared Vibrational Circular Dichroism Spectroscopy: Simulation of Real-Time Process Monitoring. *Appl. Spectrosc.* **2005**, *59*, 1114−1124.
(33) Guo, C. N.; Shah, R. D.; Mills, J.; Dukor, R. K.; Cao, X. L.; Freedman, T. B.; Nafie, L. A. Fourier Transform Near-Infrared Vibrational Circular Dichroism Used for On-Line Monitoring the Epimerization of 2,2-Dimethyl-1,3-Dioxolane-4-Methanol: A Pseudo Racemization Reaction. *Chirality* **2006**, *18*, 775−782.
(34) Nafie, L. A.; Keiderling, T. A.; Stephens, P. J. Vibrational Circular Dichroism. *J. Am. Chem. Soc.* **1976**, *98*, 2715−2723.
(35) Lakhani, A.; Malon, P.; Keiderling, T. A. Comparison of Vibrational Circular Dichroism Instruments: Development of a New Dispersive VCD. *Appl. Spectrosc.* **2009**, *63*, 775−785.
(36) Diem, M.; Roberts, G. M.; Lee, O.; Barlow, A. Design and Performance of an Optimized Dispersive Infrared Dichrograph. *Appl. Spectrosc.* **1988**, *42*, 20−27.
(37) Florkin, M., Stotz, E. H., Eds.; *Comprehensive Biochemistry*; Elsevier: Amsterdam, 1965; Vol. *6*.
(38) Kapitán, J.; Baumruk, V.; Kopecký, V.; Pohl, R.; Bouř, P. Proline Zwitterion Dynamics in Solution, Glass, and Crystalline State. *J. Am. Chem. Soc.* **2006**, *128*, 13451−13462.
(39) Marino, T.; Russo, N.; Tocci, E.; Toscano, M. Gas-Phase Acidity of Proline from Density Functional Computations. *Int. J. Quantum Chem.* **2001**, *84*, 264−268.
(40) Pecul, M.; Ruud, K.; Rizzo, A.; Helgaker, T. Conformational Effects on the Optical Rotation of Alanine and Proline. *J. Phys. Chem. A* **2004**, *108*, 4269−4276.
(41) Frisch, M. J.; Trucks, G. W.; Schlegel, H. B.; Scuseria, G. E.; Robb, M. A.; Cheeseman, J. R.; Scalmani, G.; Barone, V.; Mennucci, B.; Petersson, G. A.; et al. *Gaussian 09, Rev. B.01*; Gaussian Inc.: Wallingford, CT, 2009.
(42) Scalmani, G.; Frisch, M. J. Continuous Surface Charge Polarizable Continuum Models of Solvation. I. General Formalism. *J. Chem. Phys.* **2010**, *132*, 114110.
(43) Nafie, L. A. *Vibrational Optical Activity. Principles and Applications*; John Wiley & Sons: Chichester, 2011.
(44) Haasnoot, C. A. G.; De Leeuw, F. A. A. M.; De Leeuw, H. P. M.; Altona, C. Relationship between Proton-Proton NMR Coupling Constants and Substituent Electronegativities. III. Conformational Analysis of Proline Rings in Solution Using a Generalized Karplus Equation. *Biopolymers* **1981**, *20*, 1211−1245.
(45) Nishino, H.; Kosaka, A.; Hembury, G. A.; Matsushima, K.; Inoue, Y. The pH Dependence of the Anisotropy Factors of Essential Amino Acids. *J. Chem. Soc., Perkin Trans. 2* **2002**, 582−590.
(46) Onufriev, A.; Case, D. A.; Ullmann, G. M. A Novel View of pH Titration in Biomolecules. *Biochemistry* **2001**, *40*, 3413−3419.
(47) Varmuza, K.; Filzmoser, P. *Introduction to Multivariate Statistical Analysis in Chemometrics*; CRC Press, Taylor & Francis Group: Boca Raton, FL, 2009.
(48) Baumruk, V.; Keiderling, T. A. Vibrational Circular Dichroism of Proteins in H_2O Solution. *J. Am. Chem. Soc.* **1993**, *115*, 6939−6942.